3D Quantification of Structures in Trabecular Bone Using Measures of Complexity

Norbert Marwan*

Interdisciplinary Center for Dynamics of Complex Systems,
University of Potsdam, 14415 Potsdam, Germany
Potsdam Institute for Climate Impact Research (PIK), 14412 Potsdam, Germany

Jürgen Kurths

Department of Physics, Humboldt University Berlin, 12489 Berlin, Germany
Potsdam Institute for Climate Impact Research (PIK), 14412 Potsdam, Germany

Jesper Skovhus Thomsen

Department of Connective Tissue Biology, Institute of Anatomy,
University of Aarhus, 8000 Århus C, Denmark

Dieter Felsenberg

Charité, Campus Benjamin Franklin,
University of Medicine Berlin, 12200 Berlin, Germany

Peter Saparin†

Department of Biomaterials, Max Planck Institute of
Colloids and Interfaces, 14424 Potsdam-Golm, Germany

(Dated: October 13, 2008)

Abstract

The study of pathological changes of bone is an important task in diagnostic procedures of patients with metabolic bone diseases such as osteoporosis as well as in monitoring the health state of astronauts during long-term space flights. The recent availability of high resolution 3D imaging of bone challenges the development of data analysis techniques able to assess changes of the 3D micro-architecture of trabecular bone. We introduce a novel approach based on spatial geometrical properties and define new structural measures of complexity for 3D image analysis. These measures evaluate different aspects of organisation and complexity of 3D structures, such as complexity of its surface or shape variability. We apply these measures to 3D data acquired by high resolution micro-computed tomography (μCT) from human proximal tibiae and lumbar vertebrae at different stages of osteoporotic bone loss. The outcome is compared to the results of conventional static histomorphometry and exhibits clear relationships between the analysed geometrical features of trabecular bone and loss of bone density, but also indicate that the new measures reveal additional information about the structural composition of bone, which were not revealed by the static histomorphometry. Finally, we have studied the dependency of the developed measures of complexity on the spatial resolution of the μCT data sets.

PACS numbers: 05.45.-a, 07.05.Pj, 87.57.N-, 87.57.Q-

*Electronic address: `marwan@pik-potsdam.de`

†Electronic address: `peter.saparin@mpikg.mpg.de`

I. INTRODUCTION

Bone is a dynamic tissue that adapts its architecture to the loading conditions it is subjected to over the extent of human life. In addition, from the third decade of human life the amount of bone tissue is gradually decreasing. However, patients with osteopenia or osteoporosis, immobilised persons, or astronauts staying in micro-gravity conditions for a long period of time, may have underwent such dramatic loss of bone that they have lost a significant amount of bone stability resulting in an increased fracture risk. The changes appear as an overall loss of bone material (bone density) which is tightly coherent with a deterioration of the the micro-architecture of the interior spongy part of the bone (trabecular bone). During the last years, changes in the bone micro-structure have received much attention as the loss of bone mass alone cannot explain all variation in bone strength [1–3]. Moreover, the rapid progress in high resolution 3D micro-computed tomography (μCT) imaging facilitates the investigation of the micro-architecture of bone [4]. This new kind of high resolution 3D data requires new approaches for 3D image analysis.

The conventional method for assessing the bone status and micro-architecture is bone histomorphometry, which was developed for 2D [5] and later extended for 3D analysis [6, 7]. More recent methods for quantifying the complexity of trabecular structures derived from complexity based on symbolic dynamics [8, 9], fractal properties [10], recurrence [11], or volumetric spatial decompositions [12] have been developed. By applying these approaches to 3D images of trabecular bone, it was shown that the bone micro-architecture changes substantially during the development of osteopenia and osteoporosis. The main conclusions in [9–11] were that the complexity of the bone micro-architecture decreases with increasing bone loss and that the volume and surface of the trabecular structure changes in a different way. This latter conclusion confirms previous findings that the shape of the trabeculae changes during bone loss, e. g., from plate-like to rod-like [7].

In the present study we develop new measures of complexity for quantifying the shape and the complexity of 3D bone structures. We use 3D geometrical properties like local ratio of bone volume to bone surface and the local configuration of the neighbourhood of the bone voxel. The latter allows an assessment of the bone surface variation. We apply these measures to 3D μCT images of human proximal tibiae and vertebral bodies in order to investigate differences in trabecular bone structure at different stages of bone loss. The

available 3D μCT data sets provide for the first time a large ensemble of high quality and high resolution data of trabecular bone at different stages of osteoporosis and at different skeletal sites. We compare the results with the outcome of a conventional histomorphometrical evaluation of the same bone material. Finally, we perform an analysis based on downsampled μCT images in order to study the dependence on the image resolution and to suggest an optimal or minimal required resolution for assessment of the bone architecture.

II. MEASURES OF COMPLEXITY

The main idea behind the quantification of a geometrical shape is based on the fact that different 3D objects of the same volume have different surfaces, depending on their geometrical shape. For example, a long cylinder (length is much larger than radius) has a larger surface than a cube of the same volume, whereas a sphere has the smallest possible surface for the same given volume.

Based on the relationship between surface and shape, we introduce measures using the local bone surface and local bone volume. Because trabecular bone is a highly complex structure (cf. Figs. 6 and 7), we locally estimate the surface and volume of the trabecular bone in a small cubic box of size s, which moves without overlapping through the entire 3D image.

Surface and volume can be estimated by a simple *LEGO brick* approach (*LEGO* is a famous company that manufactures toys mainly consisting of interlocking plastic bricks) [13]: The number of voxels forming the bone structure is used as the volume, and the number of such bone voxels, which are connected to the bone marrow (surface voxels), is used as the bone surface (Fig. 1A). However, this approach is rather problematic, because, roughly speaking, the amount of surface voxels is actually not a two-dimensional surface measure as it should be, but a three-dimensional volumetric measure (after multiplying with the volume of a single voxel). Moreover, the bone volume will be overestimated when such a simple voxel counting algorithm is used. Subsequent calculations based on this simplified surface and volume estimation technique will lead to even more erroneous estimations. Therefore, in order to get more precise results, we apply an *iso-surface* algorithm to the 3D image (Fig. 1B).

An appropriate approach to construct an iso-surface is the marching cubes algorithm

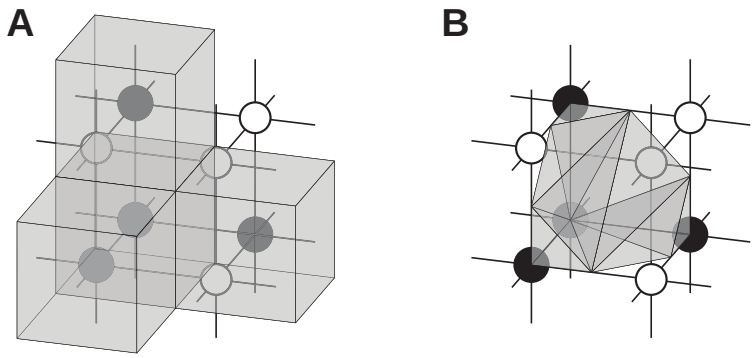

FIG. 1: A fragment of data consisting of eight voxels including four bone voxels (black nodes) and four marrow voxels (white nodes). In the *LEGO brick* approach (A), the bone surface is estimated by counting the number of bone voxels which are connected with marrow voxels (the top, front and right black nodes), and the bone volume is the number of all bone voxels. In the *iso-surface* approach (B), the surface is estimated by the sum of triangles which form an iso-surface between bone and marrow voxels; the volume is the sum of the tetrahedrons which can be filled between such iso-surface and the grid lines. The bone volume (gray shaded) will be overestimated with the *LEGO brick* approach (A), but will be calculated more precisely with the *iso-surface* approach (B).

[13, 14], which is widely used for constructing iso-surfaces in 3D data visualisation. A marching cube (MC) consists of eight neighbouring voxels. If two neighbouring voxels of this MC have voxel values above and below a predefined threshold value (i. e. one is a bone voxel and the other is a non-bone voxel), the iso-surface will lie between these two voxels. In such MC the iso-surface is formed by a set of triangles, and the surface estimation is the sum of the areas of these triangles (Fig. 1B). Now we introduce the same approach for the estimation of the bone volume. The bone volume within the MC is filled with tetrahedrons in such a way, that the resulting surface equals the iso-surface, which is formed by triangles (Fig. 2). The sum of the volumes of these tetrahedrons is the estimated bone volume contained in the MC.

For the quantification of the 3D shape, we firstly introduce the ratio between the local bone surface S_{bone} and the minimal possible surface of the given local bone volume V_{bone}, which is the surface of a sphere S_{sphere} of this volume V_{bone}. We call this ratio *local shape index* σ_{loc}. Since the local bone volume V_{bone} depends on the size of the moving box s, the normalised local bone volume $\hat{V}_{\text{bone}} = V_{\text{bone}}/s^3$ is used instead ($\hat{V}$ corresponds to the local

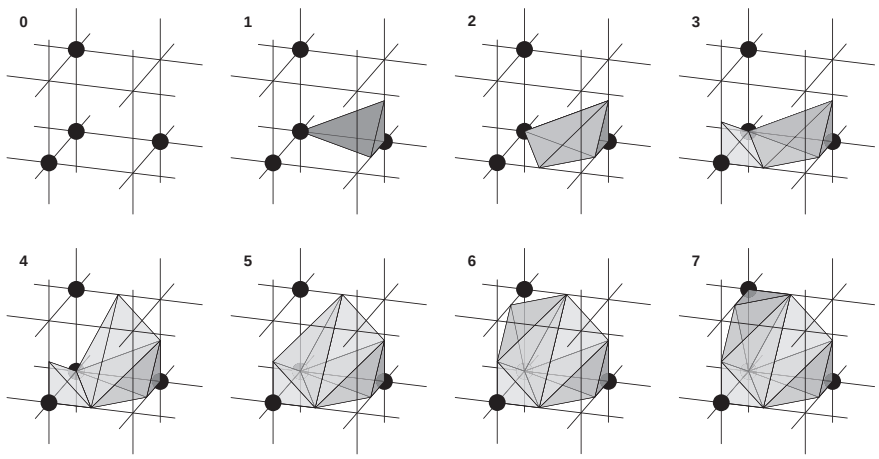

FIG. 2: Same fragment as shown in Fig. 1, which is also called marching cube. For volume estimation, the marching cube is filled with tetrahedrons constructed between the iso-surface and the grid lines.

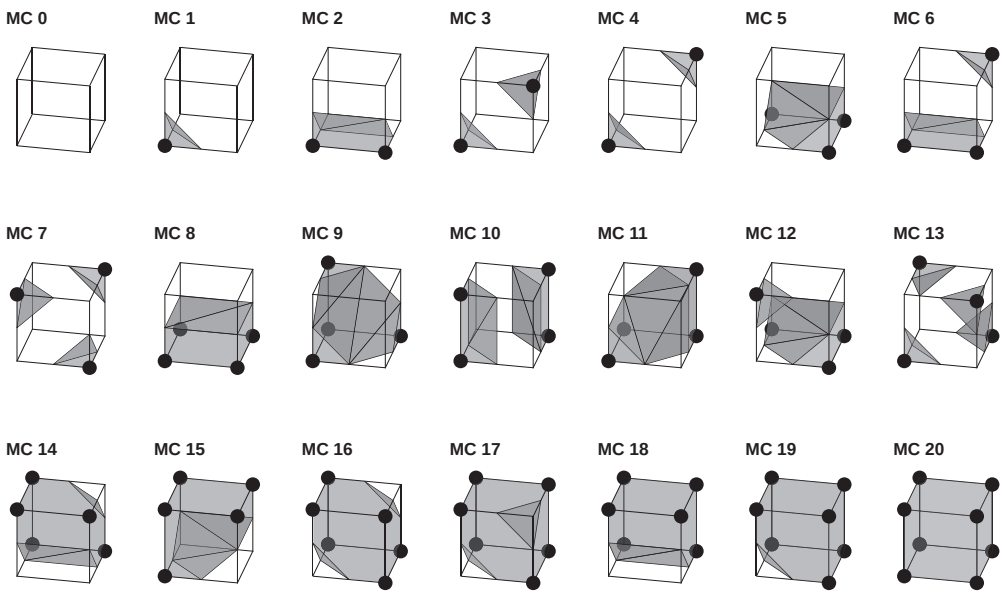

FIG. 3: The 21 pseudo-unique marching cube configurations used for defining the *marching cubes entropy index*.

bone volume fraction V_{loc}). The local shape index

$$\sigma_{\mathrm{loc}} = \frac{S_{\mathrm{bone}}}{S_{\mathrm{sphere}}} \quad \text{with} \quad S_{\mathrm{sphere}} = 6\sqrt[3]{\pi \hat{V}_{\mathrm{bone}}^2} \tag{1}$$

is able to distinguish between different shapes with the same volume but whose surface differ, like plates and rods. In principle, σ_{loc} should be equal to or larger than one, as the surface of a sphere is the smallest possible surface. However, the object could be cut by the faces of

the moving box, and as these interfaces are not included in the surface the resulting surface can be smaller than that of a sphere. Actually, this bias could be corrected by considering the cutted faces, but instead we decided to utilise this effect. This bias would mainly occur if the measured structure is concave. Therefore, σ_{loc} values less than one represent concave structures, whereas σ_{loc} values larger than one represent convex structures. Nevertheless, the size of the moving box should be as large as possible in order to reduce the effects by the cutting planes. However, the box should have such a small size that it covers only one structural element in order to get a good estimate of its shape. Therefore, the box size is a trade-off between the requests to reduce artificial effects and to increase the reliability of the estimate of the shape. We have found empirically that an optimal box size would have a size such that it covers the structural element together with its surrounding space. The box should be a little bit smaller that it just does not cover the next structural element.

Because σ_{loc} is computed within a small cubic box while moving through the studied object, we can determine a frequency distribution of the shape index over the entire object $p(\sigma_{\mathrm{loc}})$. Based on this distribution, we define the *average shape index*

$$A_\sigma = \langle \sigma_{\mathrm{loc}} \rangle_{\mathrm{VOI}}, \tag{2}$$

which is the average of all σ_{loc} in the volume of interest (VOI). A_σ measures the mean shape of the trabecular structures.

Next we define the *shape mutual information* as the mutual information between the local shape index σ_{loc} and the local bone volume fraction V_{loc}

$$I_\sigma = -\sum_{\sigma_{\mathrm{loc}}, V_{\mathrm{loc}}} p(\sigma_{\mathrm{loc}}, V_{\mathrm{loc}}) \log \frac{p(\sigma_{\mathrm{loc}}, V_{\mathrm{loc}})}{p(\sigma_{\mathrm{loc}}) p(V_{\mathrm{loc}})}. \tag{3}$$

The mutual information is a generalisation of the Shannon entropy which quantifies the dependence between two series [15]. The shape mutual information quantifies the form of the joint distribution $p(\sigma_{\mathrm{loc}}, V_{\mathrm{loc}})$ and, thus, the relationship between the local shapes of the trabecular structures and their mass. Trabecular bone with a homogeneous distribution of shapes and mass will have a joint distribution with high density in a small bounded point; i. e. the mass and shape variation are not independent, resulting in a high I_σ (Fig. 5A). For trabecular bone with a heterogeneous distribution the trabecular elements differ in shape and mass. A reduction of, e. g., plate-like elements to rod-like elements decreases both local shape index and local bone volume. Therefore, the form of the corresponding joint

distribution is stretched, but a dependence between σ_{loc} and V_{loc} still remains, resulting in a high value of I_σ (Fig. 5C). However, a higher variability of the same basic structural elements is also possible. This means that similar shapes (e. g. rod-like structures) occur with different thicknesses and thus with different bone volume fractions. Mass and shape variation are then independent. The joint distribution $p(\sigma_{\mathrm{loc}}, V_{\mathrm{loc}})$ can have the form of a normal distribution (Fig. 5B) or can be more distorted and can even exhibit several maxima (Fig. 5C). For such cases, I_σ has lower values than in the case of a homogeneous shape and mass distribution (Fig. 5A).

As another measure based on the joint distribution $p(\sigma_{\mathrm{loc}}, V_{\mathrm{loc}})$, we define the *shape complexity* as the conditional entropy of the joint distribution $p(\sigma_{\mathrm{loc}}, V_{\mathrm{loc}})$ in a given bone volume V_{loc}

$$C_\sigma = -\sum_{\sigma_{\mathrm{loc}}, V_{\mathrm{loc}}} p(\sigma_{\mathrm{loc}}, V_{\mathrm{loc}}) \log \frac{p(\sigma_{\mathrm{loc}}, V_{\mathrm{loc}})}{p(V_{\mathrm{loc}})}. \tag{4}$$

This measure quantifies the variety of different shapes for various bone volumes. If the bone surface changes in the same manner as the bone volume changes, i. e. the shape of the structure is roughly preserved, this measure will be low. However, if the bone surface is changing more dramatically and perhaps irregularly in comparison to the bone volume (i. e. shape of the structure changes), C_σ will be high.

As already mentioned, an MC is formed by eight neighbouring voxels, arranged in the shape of a cube. The entire VOI is actually a composition of many such MCs. In each MC, depending on the positions of the bone voxels, there are 256 configurations possible; neglecting rotational and inversion symmetry, there are 15 unique and fundamental MC configurations [14]. However, we will only consider rotational symmetry and ignore inversion, which result in 21 pseudo-unique MC configurations (Fig. 3). A specific marching cube configuration corresponds to a specific bone surface configuration and, hence, it is related to the complexity of the surface. For all MCs composing the VOI, we identify and count each detected MC configuration and can derive the probability $p(MC)$ with which a certain MC configuration occurs in the 3D architecture.

Since these pseudo-unique marching cube configurations (MC cases) are related to the surface complexity, we define an additional measure, the *marching cubes entropy index*

$$I_{\mathrm{MC}} = -\sum_{MC} p(MC) \log p(MC), \tag{5}$$

which is the Shannon entropy of the probability density $p(MC)$ of the MC cases, and measures the complexity of the surface of the trabecular elements. Simple complex surfaces will result in low values of I_{MC}, whereas complex surfaces will result in high values of I_{MC}.

Note that the shape complexity C_σ, shape mutual information I_σ, and marching cubes entropy index I_{MC} characterise different kinds of order in a structure. In contrast, I_{MC} assesses a global order (or disorder) of bone surfaces and C_σ and I_σ quantify the order of certain structural shapes (and for C_σ depending on the structure volume). Consequently, these measures are not necessarily correlated with each other.

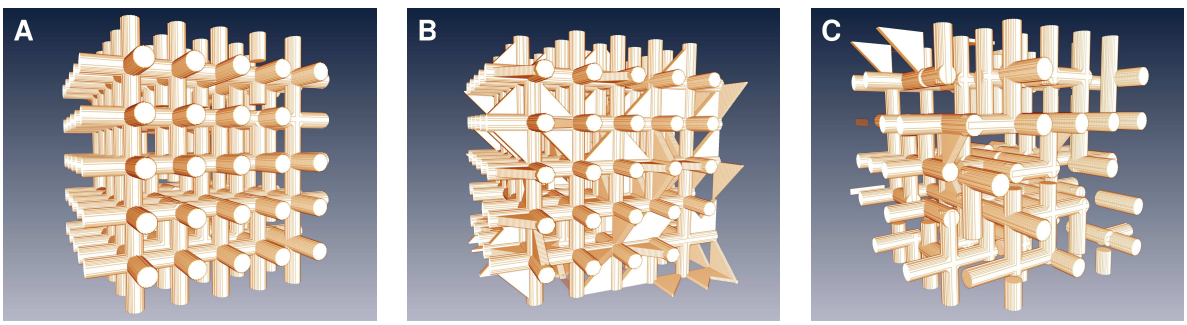

FIG. 4: (Color online) Prototypical models of a trabecular structure consisting of (A) rods, (B) plates, or (C) a deteriorated combination of rods and plates.

We illustrate the abilities of these measures on prototypical examples of 3D grids consisting of the typical structural elements of trabecular bone: rods and plates. The models have a size of $300 \times 300 \times 300$ voxels. The structural elements are periodically arranged with distances of 50 voxels in the x-, y-, and z-directions. We consider the following models:

(1) A model which is build from rods only, where 10% of the rods are removed and 10% of the rods are discontinuous. The diameter of each rod is 20 voxels (Fig. 4A).

(2) A model which is mainly build of plates; 80% of the spaces between the vertical rods is filled with plates, and 50% of the spaces between the horizontal rods is filled with plates. The thickness of each plate is 8 voxels. In order to ensure that the bone volume fraction of this model is similar to that of model (1), the diameter of the rods is scaled down to 17 voxels (Fig. 4B).

(3) Same configuration as model (2), but the probability of occurrence of plates is 10% (between vertical rods) and 1% (between horizontal rods), respectively. The diameter of each rod is 20 voxels. A deterioration of the structure is simulated by the reduced number

of plates and higher probability of removed rods (50%) and broken rods (30%) (Fig. 4C).

The amount of bone voxels, i. e. the bone volume fraction is similar for all three models.

We calculate the measures, Eqs. (2–5), based on a $50 \times 50 \times 50$ voxels moving box. Using this box size, we ensure that one structural element together with its surrounding space (up to the next structural element) will be covered by the moving box.

For the model consisting of rods only (model 1), the distribution of the local shape index σ_{loc} reveals a prominent (almost singular) peak in the distribution around a low value of σ_{loc} (Fig. 5A, vertical axis). If there were no removed or broken rods, this distribution would be a singular peak. For the model mainly consisting of plates (model 2), we find a distribution of σ_{loc} which is much wider than that for the first model (Fig. 5B). The model with the simulated deterioration has the widest distribution among the three models (Fig. 5C, vertical axis). The joint distribution between the local shape index σ_{loc} and the local bone volume fraction V_{loc} represents these behaviours more clearly. The form of the joint distribution is very different for the different structural models: it is almost singular for the rod model (1), similar to a normal distribution for the plate model (2), and stretched for the deterioration model (3) (Fig. 5). Moreover, the joint distribution for the simulated deterioration shows even several peaks, indicating the different sets of structural elements (rods, plates, broken elements).

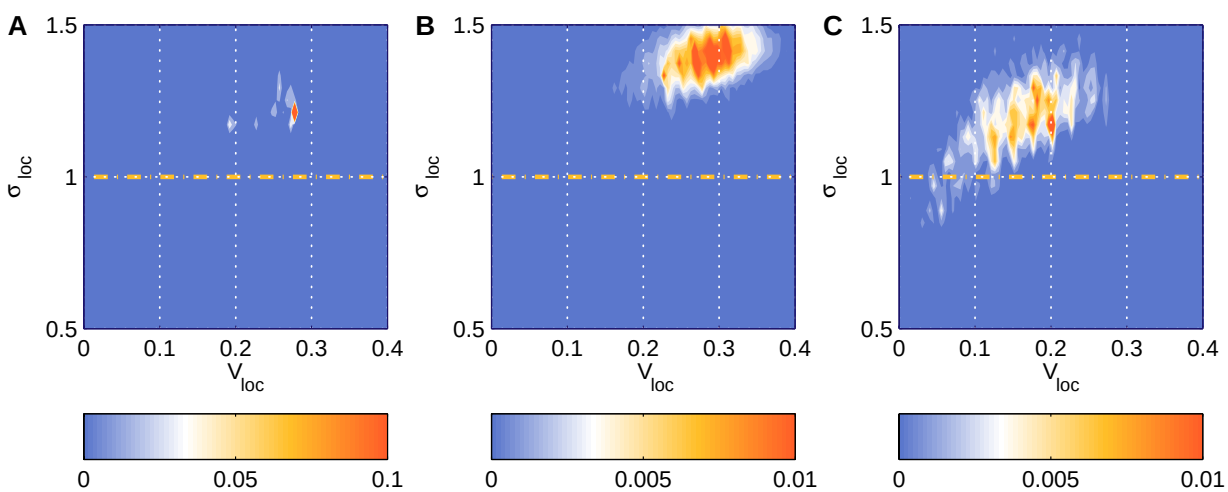

FIG. 5: (Color online) Joint distribution of local shape index σ_{loc} and the local bone volume fraction V_{loc} for the three test models consisting of (A) rods, (B) plates, and (C) a deteriorated combination of rods and plates.

TABLE I: Structural measures of complexity for the three test models consisting of rods, mainly plates, and a deteriorated combination of rods and plates.

	A_σ	I_σ	C_σ	I_{MC}
Rods	1.23	0.09	0.12	0.22
Plates	1.40	0.02	0.23	0.19
Deteriorated	1.20	0.06	0.24	0.22

The differences in the shape of the trabecular elements are quantified by our measures. The average shape index A_σ clearly distinguishes between both model configurations of plates and rods (Tab. I). As expected, the rod model has a lower value of A_σ than the plate model. The model of the simulated deterioration consists mainly of rods, but also of gaps and stumps of broken rods. Therefore, for this model we find the smallest A_σ. The variability of the shapes is quantified by the shape complexity C_σ. This measure indicates the highest shape variability for the deteriorated model and the lowest one for the rod model (Tab. I). In contrast, the complexity of the surface, as measured by the marching cubes entropy index I_{MC}, is similar for these two models (rod and deterioration model). The plate model has a lower complexity of the surface, which is not surprising due to the plates large amount of flat areas causing the same surface configuration of the marching cubes. The homogeneity of the variation of local shapes and local bone mass, as described by the joint distribution of σ_{loc} with respect to V_{loc}, is quantified by the shape mutual information I_σ. This measure indicates that the plate model is more heterogeneous than the other two models, and that the rod model is the most homogeneous of the three models. Thus, the introduced measures provide qualitative and quantitative information of the different architectural compositions. In the next section we will apply these measures to data of human trabecular bone.

III. MATERIALS

In the following the newly introduced measures, Eqs. (2–5), are used for the assessment of structural changes in trabecular bone due to osteoporotic bone loss.

29 bone specimens of proximal tibial biopsies (Fig. 6) and 18 entire L4 lumbar vertebral bodies (Fig. 7) were obtained at autopsy from the same set of donors (29 donors; for this kind of data, 29 (18) samples is a large number). The proximal tibial bone biopsies were scanned

at Scanco Medical AG (Brüttisellen, Switzerland) with a *Scanco μCT 40* micro-computed tomography scanner with an isotropic voxel size of 20 μm [16]. The vertebral bodies were scanned at Scanco Medical AG with a *Scanco μCT 80* scanner with an isotropic voxel size of 37 μm. In order to get comparable images for both skeletal sites, the data set from the proximal tibia were downsampled to a voxel size of 40 μm. The analysed set of specimens includes normal, osteopenic (initial stage of osteoporosis), and osteoporotic bones.

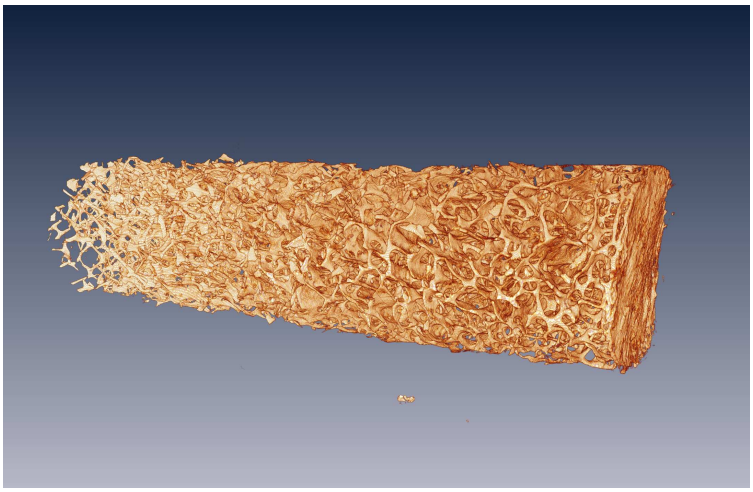

FIG. 6: (Color online) μCT scan of the cylindrical biopsy of the proximal tibia.

Standardised volumes of interest (VOI) were applied to the μCT data sets in order to quantify the 3D architecture: The VOI for the proximal tibial biopsies was located 5 mm below the cortical shell and is 10 mm long, whereas the VOI for the vertebrae was a 25 $\times$ 15 $\times$ 10 mm cuboid with the center shifted 4.5 mm backwards from the center of the vertebra along its symmetry line (Fig. 7). The results of the purposed 3D data evaluation will be compared against conventional bone histomorphometry [17]. The histomorphometry was conducted as previously described in details [16, 18]. Typical histomorphometric measures are discussed below.

IV. RESULTS

Applying the introduced measures of complexity to the VOIs of the 3D μCT data sets, we perform an evaluation of the micro-architecture of the trabecular bone of 29 proximal tibial biopsies and 18 lumbar vertebrae representing different stages of bone loss in osteoporosis. As explained in Sect. II, the size of the moving cubic box should be small enough to locally

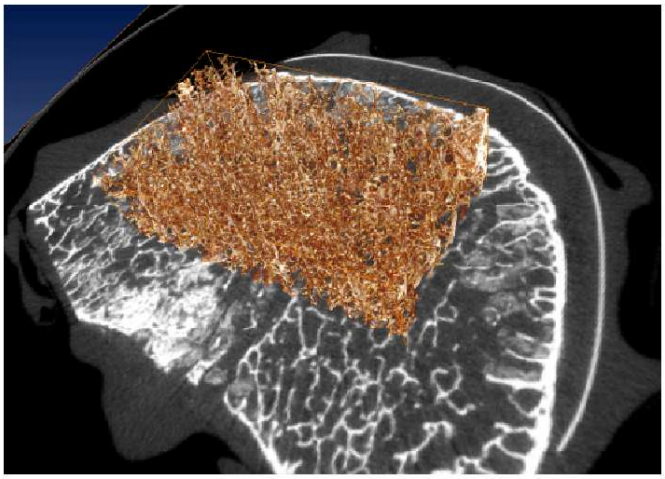

FIG. 7: (Color online) Volume of interest applied to a human lumbar vertebra. Analysed part of the trabecular structure is shown in brown, grey-scale image is the axial CT slice through the middle of the vertebral body.

quantify structural elements, but large enough to cover a sufficient surface necessary to distinguish between different shapes and to reduce artefacts. Based on this requirements, we have found empirically a trade-off for the box size to be $20\times20\times20$ voxels ($740\times740\times740$ μm) suitable for the analysis. This size equals the box size suggested for another method for structural bone analysis as proposed in [8].

Firstly, we study the joint distribution of the local shape index $\sigma_{\rm loc}$ with respect to the local bone volume $V_{\rm loc}$ (Figs. 8 and 9). These two local measures are both calculated within the moving box. Their distributions give indications about the spatial variability of the trabecular shapes and masses. The bone volume fraction, i. e. bone volume to total volume ratio, BV/TV quantifies the bone density and can be used as an indicator of bone loss. As we expect, the centre of gravity of the distribution of the local bone volume $V_{\rm loc}$ moves towards lower values during bone loss for the two different skeletal sites.

The majority of the values of the local shape index $\sigma_{\rm loc}$ is increasing during bone loss (i. e. decreasing BV/TV) in the proximal tibia. However, these values are close to and even less than one. By definition of the local shape index (1), we would expect values larger than one. The low values can be understood by considering a small piece of a trabecular structure in the proximal tibia within the moving box (Fig. 10). In contrast to a vertrebra,

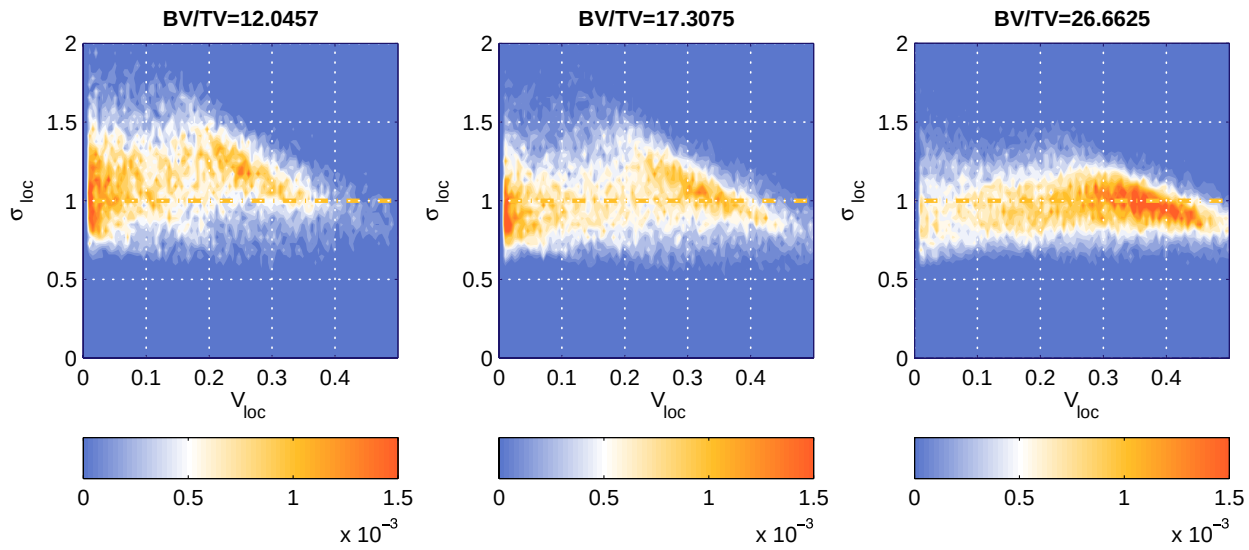

FIG. 8: (Color online) Joint distribution of the local shape index σ_{loc} and the local bone volume fraction V_{loc} for three representative μCT scans of proximal tibia biopsies.

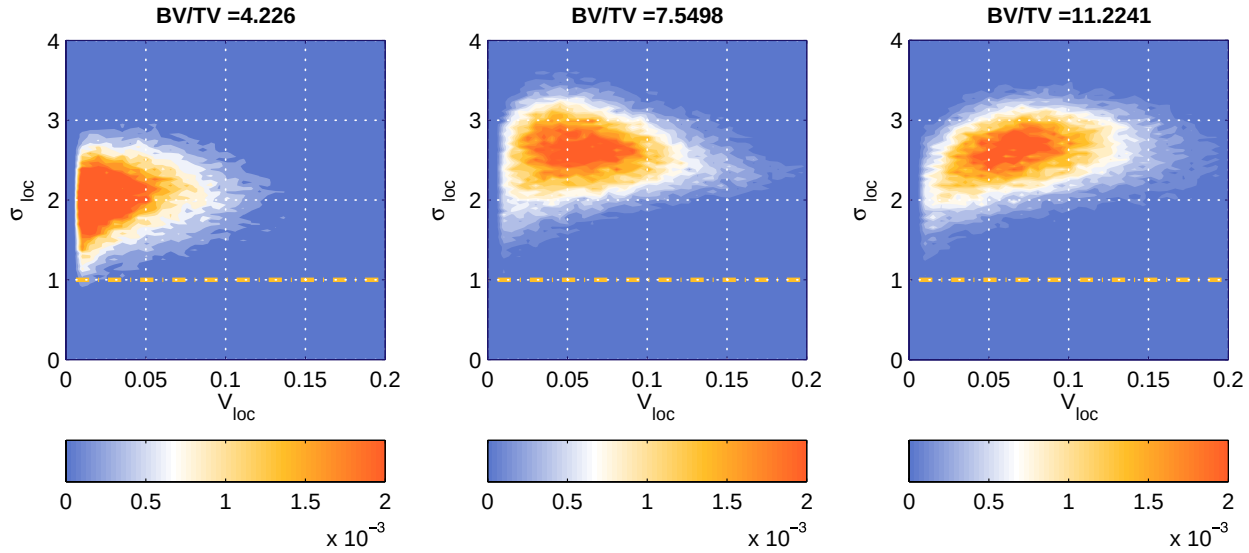

FIG. 9: (Color online) Joint distribution of the local shape index σ_{loc} and the local bone volume fraction V_{loc} for three representative μCT scans of lumbar vertebrae L4.

the trabecular bone of the proximal tibia does not consist of mainly rod-like and plate-like structures, but of more inward curving objects forming holes (Fig. 10). If the moving box covers such a cavity, the bone surface is calculated from a concave object. Consequently, the surface area may be smaller than that of a sphere of the corresponding bone volume within the moving box. This effect is an excellent indicator for concave structures. For bone loss

in proximal tibia, we find that the local shape index is increasing (at least for higher V_{loc}). This suggests a decrease of concave structures and an increase of convex structures during bone loss. Lower values of σ_{loc} occur then only for low V_{loc}, which indicates a thinning of formerly concave structures.

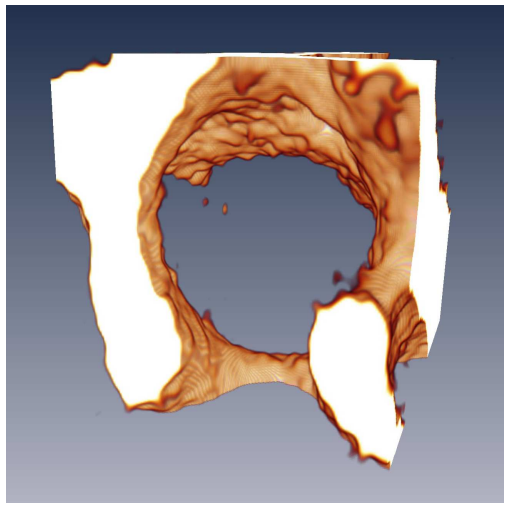

FIG. 10: (Color online) Detail of trabecular bone within the moving box. The concave structure yields to a surface which is smaller than that of a sphere of the same bone volume; hence, the corresponding local shape index will be less than one.

In contrast, the values of the local shape index σ_{loc} in the lumbar vertrebra is larger than one and decreases during bone loss. This is a clear indication of the convex nature of the vertebral trabecular micro-architecture. As plate-like structures have a higher shape index, the decrease of σ_{loc} during bone loss suggests that a significant amount of plate-like structures reduces to rod-like structures during bone loss in vertebral bodies.

Next, we use the developed approach to compare the structural changes in trabecular bone of proximal tibia and vertebral bodies caused by the bone loss in osteoporosis (Fig. 11). As an indicator of bone loss, we use the bone volume fraction BV/TV as derived from histomorphometry. Again, we find some remarkable differences between the proximal tibia and the lumbar vertebra.

During bone loss, the averaged shape index A_σ decreases in the vertebra, but increases in the proximal tibia (Fig. 11A). Moreover, for high density proximal tibiae (BV/TV $> 20\%$) its values are below one. This confirms our previous findings that normal trabecular bone in the proximal tibia contains a large number of concave structures. Bone loss causes a

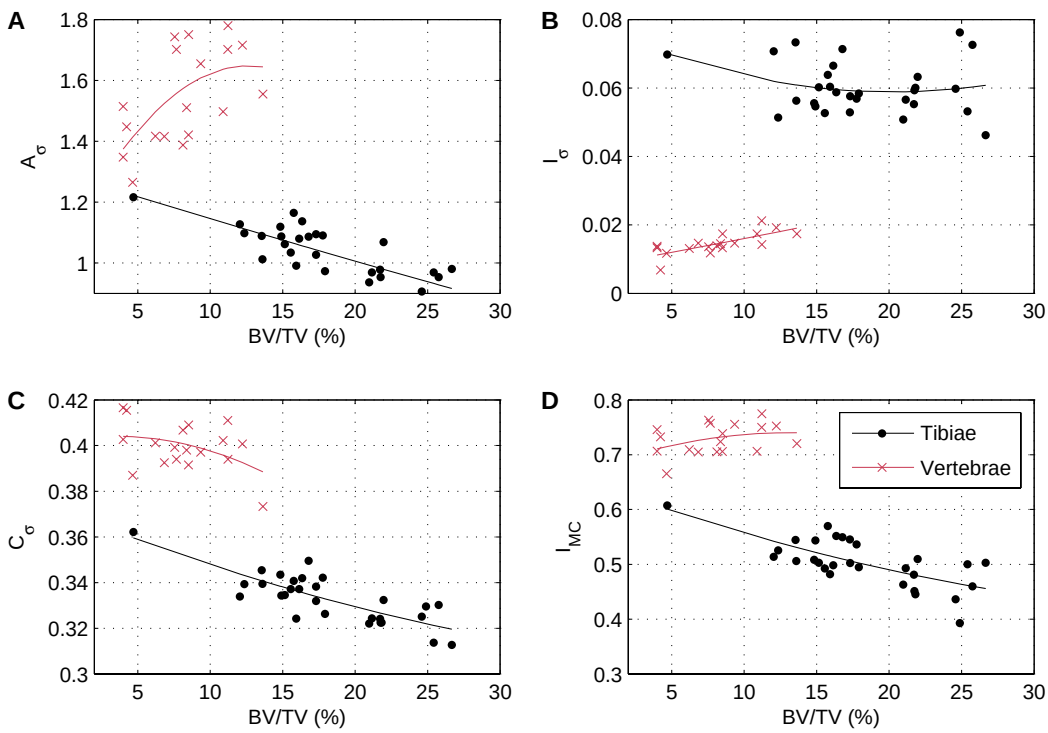

FIG. 11: (Color online) Measures of complexity vs. bone loss (represented by bone volume fraction BV/TV) for proximal tibiae (dots) and lumbar vertebrae (crosses). The lines are polynomial fits of 2nd order to guide the eye.

shift from concave structures to convex structures. A_σ for vertebra is greater than one. The Spearman's rank correlation coefficient between BV/TV and A_σ is $R = -0.75$ ($p < 0.01$) for proximal tibia and $R = 0.57$ (n. s.) for vertebra.

The shape mutual information I_σ does not depend on the different stages of bone loss in the proximal tibia. In contrast, I_σ shows a clear linear correlation with bone loss for the vertebra (Fig. 11B). Moreover, the values of I_σ are considerably higher for the proximal tibia than for the vertebra. These findings suggest that the variability of the shapes of the trabecular elements is higher in the vertebra than in the proximal tibia. Furthermore, the change of the structural shape of the trabeculae is different at these two skeletal sites. In vertebrae the trabeculae change from a given set of shapes to another set of shapes (plate-like to rod-like structures) during bone loss, whereas in proximal tibiae the shape of the structures do not undergo such a well defined transition during bone loss. An explanation for this could be that proximal tibial trabecular bone has a more homogeneous and less

complex micro-architecture than vertebral trabecular bone.

The shape complexity C_σ reveals the same trend for both proximal tibia and vertebra (Fig. 11C). During bone loss, the variety of the shapes of the trabecular elements increases. This variability is higher in the vertebrae than in the proximal tibiae. I_{MC} reveals a tendency similar to that of A_σ: anti-correlation for the proximal tibia, but weak correlation for the lumbar vertebra (Fig. 11D). However, the correlations are only significant for the proximal tibia. From the correlation between I_{MC} and BV/TV we infer that in the vertebrae the complexity of the bone surface decreases during bone loss, whereas in the proximal tibia the complexity of the bone surface increases during bone loss. However, this effect is not as pronounced for vertebral bone as it is for tibial bone.

Next, we compare the introduced structural measures of complexity with some of the classical histomorphometrical measures (Tab. II, Fig. 12). We find that the majority of these measures are significantly correlated to the measures of complexity at the proximal tibia only (except I_σ). This is probably due to a higher variability of the shapes over the vertebral bodies and selection of only one region for histomorphometric analysis.

The trabecular separation Tb.Sp measures the mean trabecular plate separation under the assumption that the bone tissue is distributed as parallel plates [5]. In trabecular bone, consisting of emphasised and clear rod-like and plate-like structures, as in the vertebra, a variation of these structures should be measured by Tb.Sp and also on shape index based meaures. At the vertebral body A_σ and I_σ are significantly correlated with Tb.Sp, whereas at the proximal tibia only C_σ is correlated with Tb.Sp.

The nodes-termini ratio Nd/Tm represents the connectivity of the network as it appears on a 2D section [19]. A change in the connectivity of the network causes a change in the complexity of the bone surface. Therefore, at the proximal tibia we find that Nd/Tm is strongly correlated with I_{MC}. At the vertebral body Nd/Tm and I_{MC} are also correlated, but this correlation does not reach the level of significance.

A further histomorphometric measure, which characterises the trabecular network, is the trabecular bone pattern factor TBPf [20]. Similar to Nd/Tm, this measure is up to some account related to the complexity of the trabecular bone surface. We find that TBPf is, like Nd/Tm, strongly related with the suggested measures of complexity, in particular with I_{MC}. Again, for vertebrae these correlations are not significant (except for I_σ).

These results confirm that the averaged shape index A_σ, the shape mutual information I_σ,

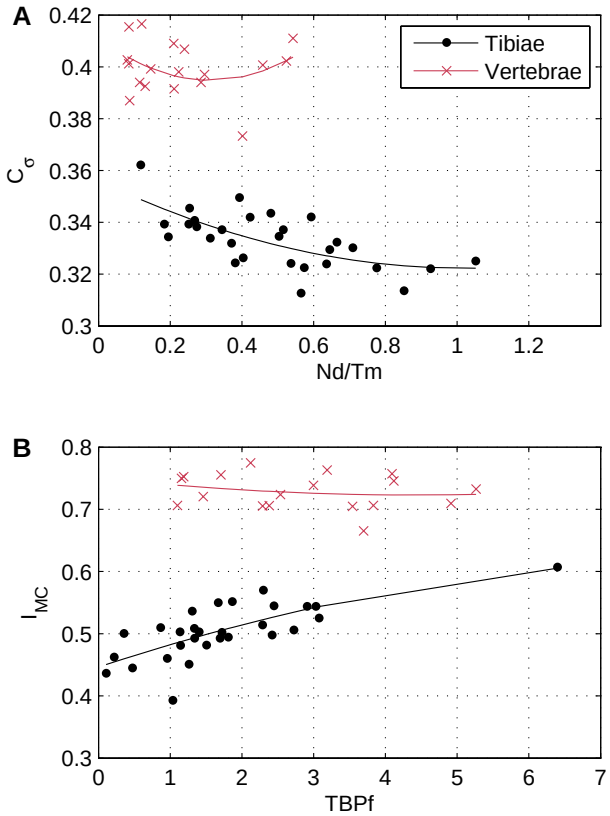

FIG. 12: (Color online) Measures of complexity vs. node-terminus ratio (Nd/Tm) and trabecular bone pattern factor (TBPf) for proximal tibiae (dots) and lumbar vertebrae (crosses). The lines are squared fits to guide the eye.

the shape complexity C_σ, and the marching cubes entropy index I_{MC} assess the shape and complexity of the trabecular micro-architecture. The ability to quantify architecture as well as the different aspects of the introduced measures of complexity are clearly illustrated at the proximal tibia and vertebra by comparing the micro-architecture of the trabecular bone at these two skeletal sites. We have demonstrated quantitatively that the architecture of lumbar vertebral trabecular bone is very different from proximal tibial trabecular bone by use of the new structural measures. Since this difference is less pronounced for the histomorphometric measures we therefore infer that these introduced structural measures reveal additional information about the bone structure, which are not included in the histomorphometric measures. In addition, our results confirm the well-known structural differences of different skeletal sites [21–23].

The relationships we found between the developed measures and the bone architecture as

TABLE II: Spearman's rank correlation coefficients between structural measures of complexity and bone volume fraction as well as histomorphometrical measures. Statistically significant values ($p = 0.01$) are black, non-significant values are gray.

	A_σ	I_σ	C_σ	I_{MC}
Proximal Tibiae				
BV/TV	−0.75	−0.08	−0.72	−0.61
Tb.Sp	0.45	0.26	0.58	0.35
Nd/Tm	−0.72	−0.05	−0.65	−0.71
TBPf	0.72	0.09	0.66	0.69
Lumbar Vertebrae				
BV/TV	0.57	0.78	−0.27	0.31
Tb.Sp	−0.71	−0.81	0.26	−0.44
Nd/Tm	0.38	0.81	−0.07	0.17
TBPf	−0.35	−0.82	0.14	−0.11

well as the relationships between the structural complexity measures and the histomorphometric measures suggest that the proposed new measures of complexity are able to quantify 3D bone architecture. In addition, they contain important information about the trabecular geometry and can be used to describe changes in the spatial structure of trabecular bone.

V. SENSITIVITY TEST

In order to study the sensitivity of the developed complexity measures to the voxel size of the CT images and to find a minimal required voxel size (or image resolution) for the application of the introduced measures of complexity, we use the available 18 μCT scans of lumbar vertebra including normal, osteopenic, and osteoporotic specimens (as described in Sect. III).

In a computer experiment we simulate that the vertebrae were scanned with different lower resolutions (i. e. larger voxel sizes). To simplify the notion we assume that the resolution of the 3D image is only defined by its voxel size. For this purpose we downsample the data sets using a Lanczos kernel [24]. For example, a resampling to two times larger

voxel size means a decreasing of the resolution by 50%. In order to compare the different resolutions, we resample the downsampled data back to the original resolution and assess the resulting data sets with the complexity measures. The VOI is the same as for the original resolution: a vertical cuboid of size $10 \times 10 \times 25$ mm in the centre of the vertebra. We downsample the μCT images to 10% to 90% of the original size (with steps of 5 percent points between 10% and 50% and with steps of 10 percent points between 50% and 90%). These values correspond to a reduced resolution, or higher voxel size. Because of the original voxel size of $S = 37$ μm, the voxel size $S(d)$ of the simulated new CT image can be calculated as $S(d) = 37$ μm$/d$, where d is the downsampling ratio. E. g., for a downsampling of $d = 50\%$ $= 0.05$ we have a corresponding voxel size of $S = 74$ μm. The size of the moving box is as in Sect. IV $20 \times 20 \times 20$ voxels for all downsampling stages.

The introduced complexity measures show a more-or-less linear dependence on the image resolution between 40% and 90% of the original resolution (Fig. 13). For decreasing resolution, the values of these measures decrease as well. However, for resolutions smaller than 30% of the original resolution, the values decrease more dramatically, especially for A_σ, C_σ, and I_{MC}. Moreover, the values come closer to each other, preventing a clear discrimination of the different architecture of the samples. The values of I_σ strongly increase for very low resolutions. For I_{MC} we find a critical change in the values resulting in an alteration of the order of the samples (crossing of the curves in Fig. 13D).

In order to quantify the differences in the measures of complexity due to the resolution, we compute the Spearman's rank correlation coefficient between the complexity measures

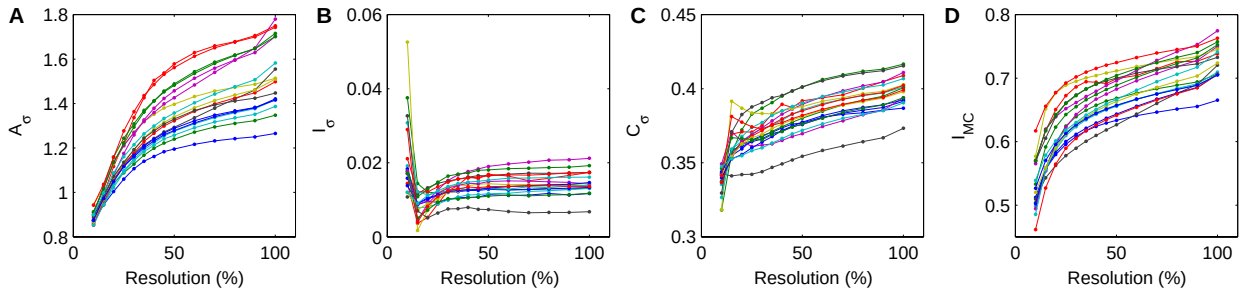

FIG. 13: (Color online) Measures of complexity of the μCT images of lumbar vertebrae L4 (different curves) for different simulated image resolutions (given in percentage of the original image resolution).

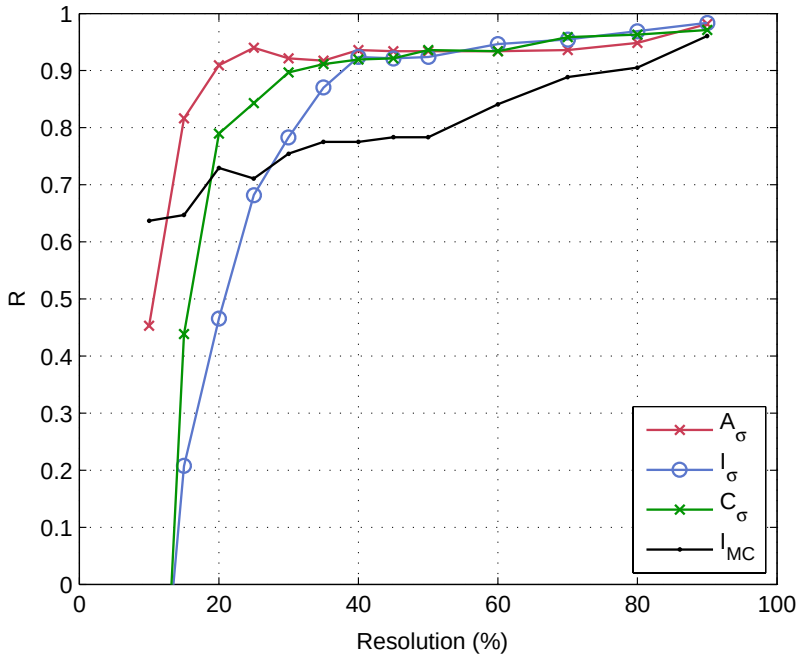

FIG. 14: (Color online) Spearman's rank correlation R between the complexity measures derived from μCT images of lower resolutions and the complexity measures derived from using the original resolution.

of the original data and the complexity measures of the lower resolution (Fig. 14).

In this way we can estimate the minimal possible resolution necessary to obtain results that are comparable to those obtained at the original resolution (which could be further improved in the future by the technological progress). Applying a threshold of $R = 0.9$, we find that for the averaged shape index A_σ the minimal required resolution is 20% of the original resolution, corresponding to a voxel size of 185 μm, for the shape mutual information I_σ it is 40% (93 μm), for the shape complexity C_σ, it is 35% (104 μm), and, due to its high sensitivity, for the marching cubes entropy index I_{MC} the minimal resolution is 80% of the original resolution, corresponding to 46 μm.

VI. CONCLUSION

In the present study we have introduced a series of new measures of complexity for structural analysis of 3D data sets and tested their ablities on prototypical model systems. Using the introduced measures, we have been able to establish significant differences in 3D bone

TABLE III: Summarised main results (differences and change under bone loss) found for proximal tibia and lumbar vertebra; ↓– property decreases during bone loss, ↑– property increases during bone loss, and →– property does not change much during bone loss.

	proximal tibia	lumbar vertebra
bone density (BV/TV)	higher ↓	lower ↓
shape of trabecular elements (A_σ)	concave and convex, amount of concave elements ↓	mainly convex →
shape distribution of trabecular elements/ homogenity (I_σ)	more homogeneous →	less homogeneous ↓
shape variability of trabecular elements (C_σ)	lower than in lumbar vertebra ↑	higher than in proximal tibia ↑
complexity of bone surface (I_{MC})	lower ↑	higher ↓

architecture at different levels of bone loss including osteopenia and osteoporosis at the proximal tibia and lumbar vertrebra (Tab. III). Furthermore, we found that proximal tibial trabecular bone contains more concave structural elements than lumbar vertrebral trabecular bone. Moreover, the amount of concave structures decreases during bone loss, while the proportion of convex structures increases. In addition, the complexity of the bone surface is decreasing during bone loss in lumbar vertebral trabecular bone, whereas it is increasing in proximal tibial trabecular bone. Although the complexity of the trabecular bone structure is higher in healthy bone, the complexity of the shapes of local structural elements dependency on its volume is lower in healthy bone. This means that osteoporotic structural elements of a given volume have a higher variability in the shape than healthy bone. Furthermore, we have found that the new measures reveal additional information about the structural composition, which were not obtained by the measures of static histomorphometry.

Based on computer simulations, we studied the sensitivity of the introduced measures on the voxel size. The measures based on the shape index (A_σ, I_σ, and C_σ) are less sensitive to increases in voxel size, whereas the marching cubes based measure (I_{MC}) is much more sensitive to increases in voxel size.

The proposed new structural measures of complexity can be directly computed from 3D images and, thus, are non-invasive and non-destructive. They convey important and

additional information about the 3D structure of trabecular bone and can be used to describe the deterioration of the trabecular bone network that takes place during the development of osteopenia and osteoporosis. Although high resolution 3D images are preferable, these measures can be applied on 3D images of lower resolution as obtained in vivo. First tests on patients have already revealed promising results. Moreover, as there is an ongoing process of technological improvements in the CT technology, we can expect higher resolution micro-CTs even for in vivo imaging in the next years. Furthermore, our measures are also a promising approach for the investigation of other complex 3D structures of different origin, like ceramic foam.

Acknowledgments

This study was made possible in part by grants from the Microgravity Application Program/ Biotechnology from the Human Spaceflight Program of the European Space Agency (project MAP AO-99-030) and support from Siemens AG and Scanco Medical AG. Scanco Medical AG is gratefully acknowledged for μCT scanning the bone samples. We appreciate the great support we received from Gottfried Bogusch, Charité Berlin, Campus Mitte, for providing the bone specimens. Erika May and Wolfgang Gowin, Charité Berlin, Campus Benjamin Franklin, are gratefully acknowledged for preparing the bone samples. Inger Vang Magnussen, University of Aarhus, is acknowledged for preparing the bone samples for histomorphometry. We thank Hans-Chrisian Hege and Steffen Prohaska, Zuse Institute Berlin (ZIB), for the support and help with the Amira software, as well as Wolfgang Gowin for fruitful discussions.

[1] J. S. Thomsen, E. N. Ebbesen, and L. Mosekilde, Bone **30**, 502 (2002), doi: 10.1016/S8756-3282(01)00702-5.

[2] L. A. Feldkamp, S. A. Goldstein, A. M. Parfitt, G. Jesion, and M. Kleerekoper, Journal of Bone and Mineral Research **4**, 3 (1989).

[3] D. Ulrich, B. van Rietbergen, A. Laib, and P. Rüegsegger, Bone **25**, 55 (1999), doi: 10.1016/S8756-3282(99)00098-8.

[4] D. W. Holdsworth and M. M. Thornton, Trends in Biotechnology **20**, 34 (2002), doi: 10.1016/S0167-7799(02)02004-8.

[5] A. M. Parfitt, C. H. E. Mathews, A. R. Villanueva, M. Kleerekoper, B. Frame, and D. S. Rao, Journal of Clinical Investigation **72**, 1396 (1983), doi: 10.1172/JCI111096.

[6] M. Ito, T. Nakamura, T. Matsumoto, K. Tsurusaki, and K. Hayashi, Bone **23**, 163 (1998), doi: 10.1016/S8756-3282(98)00083-0.

[7] T. Hildebrand, A. Laib, R. Müller, J. Dequeker, and P. Rüegsegger, Journal of Bone and Mineral Research **14**, 1167 (1999), doi: 10.1359/jbmr.1999.14.7.1167.

[8] P. I. Saparin, W. Gowin, J. Kurths, and D. Felsenberg, Physical Review E **58**, 6449 (1998), doi: 10.1103/PhysRevE.58.6449.

[9] P. I. Saparin, J. S. Thomsen, S. Prohaska, A. Zaikin, J. Kurths, H.-C. Hege, and W. Gowin, Acta Astronautica **56**, 820 (2005), doi: 10.1016/j.actaastro.2005.01.007.

[10] N. Marwan, P. Saparin, and J. Kurths, The European Physical Journal – Special Topics **143**, 109 (2007), doi: 10.1140/epjst/e2007-00078-x.

[11] N. Marwan, J. Kurths, and P. Saparin, Physics Letters A **360**, 545 (2007), doi: 10.1016/j.physleta.2006.08.058.

[12] M. Stauber and R. Müller, Bone **38**, 475 (2006), doi: 10.1016/j.bone.2005.09.019.

[13] T. T. Elvins, ACM SIGGRAPH Computer Graphics **26**, 194 (1992), doi: 10.1145/142413.142427.

[14] W. E. Lorensen and H. E. Cline, ACM SIGGRAPH Computer Graphics **21**, 163 (1987), doi: 10.1145/37402.37422.

[15] A. M. Fraser and H. L. Swinney, Physical Review A **33**, 1134 (1986), doi: 10.1103/PhysRevA.33.1134.

[16] J. S. Thomsen, A. Laib, B. Koller, S. Prohaska, L. Mosekilde, and W. Gowin, Journal of Microscopy **218**, 171 (2005), doi: 10.1111/j.1365-2818.2005.01469.x.

[17] J. S. Thomsen, E. N. Ebbesen, and L. Mosekilde, Bone **27**, 129 (2000), doi: 10.1016/S8756-3282(00)00285-4.

[18] P. Saparin, J. S. Thomsen, J. Kurths, G. Beller, and W. Gowin, Medical Physics **33**, 3857 (2006), doi: 10.1118/1.2336501.

[19] N. J. Garrahan, R. W. E. Mellish, and J. E. A. Compston, Journal of Microscopy **142**, 341 (1986).

[20] M. Hahn, M. Vogel, M. Pompesius-Kempa, and G. Delling, Bone **13**, 327 (1992), doi: 10.1016/8756-3282(92)90078-B.

[21] O. M. Pearson and D. E. Lieberman **125**, 63 (2004), doi: 10.1002/ajpa.20155.

[22] P. Saparin, W. Gowin, and D. Felsenberg, Journal of Gravitational Physiology **9**, 177 (2002).

[23] J. S. Thomsen, E. N. Ebbesen, and L. Mosekilde, Bone **30**, 267 (2002), doi: 10.1016/S8756-3282(01)00666-4.

[24] T. M. Lehmann, C. Gönner, and K. Spitzer, IEEE Transactions on Medical Imaging **18**, 1049 (1999), doi: 10.1109/42.816070.